OXFORD

Human Molecular Genetics, 2016, Vol. 25, No. 21 4771–4786

doi: 10.1093/hmg/ddw304
Advance Access Publication Date: 30 August 2016
Original Article

ORIGINAL ARTICLE

Sex-dependent effects of chromogranin B P413L allelic variant as disease modifier in amyotrophic lateral sclerosis

Yasuyuki Ohta[1,2], Genevieve Soucy[1,2], Daniel Phaneuf[1,2], Jean-Nicolas Audet[1,2], François Gros-Louis[3], Guy A. Rouleau[4], Hélène Blasco[5], Philippe Corcia[5], Peter M. Andersen[6,7], Frida Nordin[6], Toru Yamashita[8], Koji Abe[8] and Jean-Pierre Julien[1,2,*]

[1]Research Centre of Institut universitaire en santé mentale de Québec, Québec, QC, Canada, [2]Department of Psychiatry and Neuroscience, Laval University, Québec, QC, Canada, [3]CHU de Québec Research Center, LOEX Hôpital de l'Enfant-Jésus, Quebec, QC, Canada, [4]Montreal Neurological Institute, McGill University, Montreal, QC, Canada, [5]Centre de Ressources et Compétences SLA (CRCSLA), Federation des CRCSLA Tours-Limoges LITORALS, INSERM U 930, Université François-Rabelais de Tours, France, [6]Department of Pharmacology and Clinical Neuroscience, Umeå University, Umeå, Sweden, [7]Department of Neurology, Ulm University, Ulm, Germany and [8]Department of Neurology, Graduate School of Medicine, Dentistry and Pharmaceutical Sciences, Okayama University, Okayama, Japan

*To whom correspondence should be addressed at: Jean-Pierre Julien, Research Centre of Institut universitaire en santé mentale de Québec, 2601 Chemin de la Canardière Québec, QC, G1J 2G3, Canada. Tel: 418 663-5000 ext 4785; Fax: 418-663-5971; Email: jean-pierre.julien@fmed.ulaval.ca

Abstract

Recent genetic studies yielded conflicting results regarding a role for the variant chromogranin B (CHGB)^{P413L} allele as a disease modifier in ALS. Moreover, potential deleterious effects of the CHGB^{P413L} variant in ALS pathology have not been investigated. Here we report that in transfected cultured cells, the variant CHGB^{L413} protein exhibited aberrant properties including mislocalization, failure to interact with mutant superoxide dismutase 1 (SOD1) and defective secretion. The CHGB^{L413} transgene in SOD1^{G37R} mice precipitated disease onset and pathological changes related to misfolded SOD1 specifically in female mice. However, the CHGB^{L413} variant also slowed down disease progression in SOD1^{G37R} mice, which is in line with a very slow disease progression that we report for a Swedish woman with ALS who is carrier of two mutant SOD1^{D90A} alleles and two variant CHGB^{P413L} and CHGB^{R458Q} alleles. In contrast, overexpression of the common CHGB^{P413} allele in SOD1^{G37R} mice did not affect disease onset but significantly accelerated disease progression and pathological changes. As in transgenic mice, the CHGB^{P413L} allele conferred an earlier ALS disease onset in women of Japanese and French Canadian origins with less effect in men. Evidence is presented that the sex-dependent effects of CHGB^{L413} allelic variant in ALS may

Received: June 1, 2016. **Revised:** July 28, 2016. **Accepted:** August 25, 2016

arise from enhanced neuronal expression of *CHGB* in females because of a sex-determining region Y element in the gene promoter. Thus, our results suggest that *CHGB* variants may act as modifiers of onset and progression in some ALS populations and especially in females because of higher expression levels compared to males.

Introduction

Amyotrophic lateral sclerosis (ALS) is an adult-onset neurodegenerative disorder characterized by the progressive loss of motor neurons. Most ALS patients die within 2 to 5 years after onset of symptoms since no effective treatment exists. Approximately 90% of ALS cases are sporadic. The most frequent genetic causes of familial ALS are mutations in the gene coding for superoxide dismutase 1 (SOD1) (1,2) and an expansion of hexanucleotide repeats in noncoding region of *C9ORF72* (3,4). Rare mutations in many disparate genes including *TARDBP*, *TBK1*, *NEK1*, *FUS*, *ALS2*, *DCTN1*, *SETX*, *VAPB*, *VEGF*, *ANG*, *CHMP2B*, *VCP*, *OPTN*, *PFN1*, *SQSTM1* and *UBQLN2* are also known to be associated with ALS (5–26).

Chromogranins, which are major constituents of secretory large dense-core vesicles in neurons, act as chaperone-like proteins that bind mutant SOD1 proteins to promote their secretion (27). This finding led us to search for chromogranin genetic variations in ALS and control subjects. A few years ago we reported that a common chromogranin B (CHGB)^{P413L} variation was associated with higher risk to develop ALS and with earlier age of onset in both sporadic and familial ALS cases in cohorts of French-Canadian origin (28). However, these results have not been corroborated by other groups that reported a lack of association of *CHGB*^{P413L} with ALS in other populations from the Netherlands, France and Italy (29–31). Although the divergent results might be explained by population-specific effects, a pathogenic role for the CHGB^{P413L} variant in ALS remains unknown.

Here, we demonstrate a mislocalization and defective binding and secretion of CHGB^{L413} variant for mutant and misfolded SOD1 in transfected cultured cells. We generated transgenic mice bearing genomic fragments coding for the human CHGB^{L413} or CHGB^{P413} variants to derive double transgenic SOD1^{G37R} mice co-expressing mutant SOD1 and CHGB variants. The expression of the CHGB^{L413} transgene in SOD1^{G37R} mice caused an earlier disease onset and pathological changes specifically in female mice. As in transgenic mice, the sex-dichotomous effects of the CHGB^{P413L} variant on the onset of ALS were also observed in ALS cohorts of Japanese and French-Canadian origins. Evidence is presented that the sex-dichotomous effects of a CHGB^{L413} allele in ALS are related to enhanced gene expression in females due to a sex-determining region Y (SRY) silencer element in the *CHGB* promoter.

Results

Defective binding properties of CHGB^{P413L} and CHGB^{H230R} protein variants

We previously reported that mouse chromogranins can interact with mutant or oxidized SOD1 *in vitro* (27,32). Thus, we investigated the effect of amino acid variation in CHGB^{L413} on the ability to bind mutant SOD1. In these studies, we also included another rare chromogranin variant, CHGB^{R230}, detected only in few ALS cases but not in control individuals (28). We carried out transient co-expression assays in Neuro2a cells using plasmid vectors coding for mouse chromogranin B (mCgB) or various human CHGB species tagged with hemagglutinin (HA) at the carboxy terminus together with vectors coding for wild type (WT) or SOD1^{G93A} species tagged with FLAG at the amino terminus. As shown in Figure 1A, after co-transfection of vectors in Neuro2a cell, the immunoprecipitation of mutant SOD1^{G93A}, but not WT SOD1, with anti-FLAG in cell extracts led to co-precipitation of mouse mCgB or of human CHGB WT (P413/H230). In contrast, the variants CHGB^{L413} and CHGB^{R230} were not co-immunoprecipitated with SOD1^{G93A}. To further confirm the failure of CHGB^{L413} to interact with mutant SOD1, we carried out transient co-expression assays in Neuro2a cells of FLAG-SOD1^{G93A} with vectors bearing genomic fragments coding for CHGB$^{P413/H230}$ (WT) or variant CHGB^{L413}. The genomic CHGB fragments included 5.1 kb of CHGB promoter region and 13.7 kb of exon/intron sequences (Fig. 1B). Total cell lysates from transfected cells were fractionated by two-dimensional gel electrophoresis and then transferred to a membrane for immunodetection of CHGB. As shown in Supplementary Material, Figure S1A, WT CHGB$^{P413/H230}$ was co-immunoprecipitated with mutant SOD1^{G93A} whereas the variant CHGB^{L413} failed to co-immunoprecipitate with mutant SOD1^{G93A}.

Additional evidence of defective binding of CHGB variants (L413 and R230) with mutant SOD1 or misfSOD1 was obtained by immunofluorescence confocal microscopy of Neuro2a cells after transfection of vectors encoding mouse CgB or human CHGB variants with SOD1 species. The WT SOD1, mainly a cytosolic protein, did not co-localize with CgB or CHGB species (Fig. 1C, Supplementary Material, Fig. S1B). However, the subcellular distribution of mutant SOD1^{G93A} or misfolded SOD1 (misfSOD1) stained by B8H10 antibody in Neuro 2A cells was altered by the co-expression of mouse CgB or WT CHGB$^{P413/H230}$. Thus, SOD1^{G93A} or mifSOD1 was partially immunodetected with CgB or WT CHGB$^{P413/H230}$ in Neuro2A cells (Fig. 1C and D, Supplementary Material, Fig. S1B and C). A total colocalization of SOD1^{G93A} and mifSOD1 with WT CHGB$^{P413/H230}$ was observed in 14.7% and 13.6% of doubly transfected Neuro2a cells, respectively. In contrast, the mutant SOD1^{G93A} or misfSOD1was not co-localized with the variants CHGB^{L413} and CHGB^{R230} (Fig. 1C and D).

Mislocalization and defective secretion of CHGB^{L413} and CHGB^{R230} variants in cultured cells

To further investigate the localization of CHGB WT and variants in the context of overexpression of human SOD1 species, Neuro2a cells were co-transfected with HA-CHGB species and FLAG-SOD1 species, and then analyzed by double immunofluorescence using antibodies against trans-Golgi marker (TGN38) or synaptic vesicle marker (synaptophysin). Confocal laser microscopy revealed that a large fraction of HA-CHGB WT (67%) was detected with the trans-Golgi marker in cells transfected with HA-CHGB WT alone (Fig. 2A). The co-transfection of SOD1^{G93A} vector reduced the detection of HA-CHGB WT with the trans-Golgi marker (56%) (Fig. 2A). Synaptic vesicle markers were located diffusely and partially accumulated in the cytoplasm of Neuro2a cells. Some of the HA-CHGB WT was co-localized with the accumulation of synaptic vesicle marker in cells co-transfected with SOD1^{G93A} (Fig. 2B, arrowheads). It is

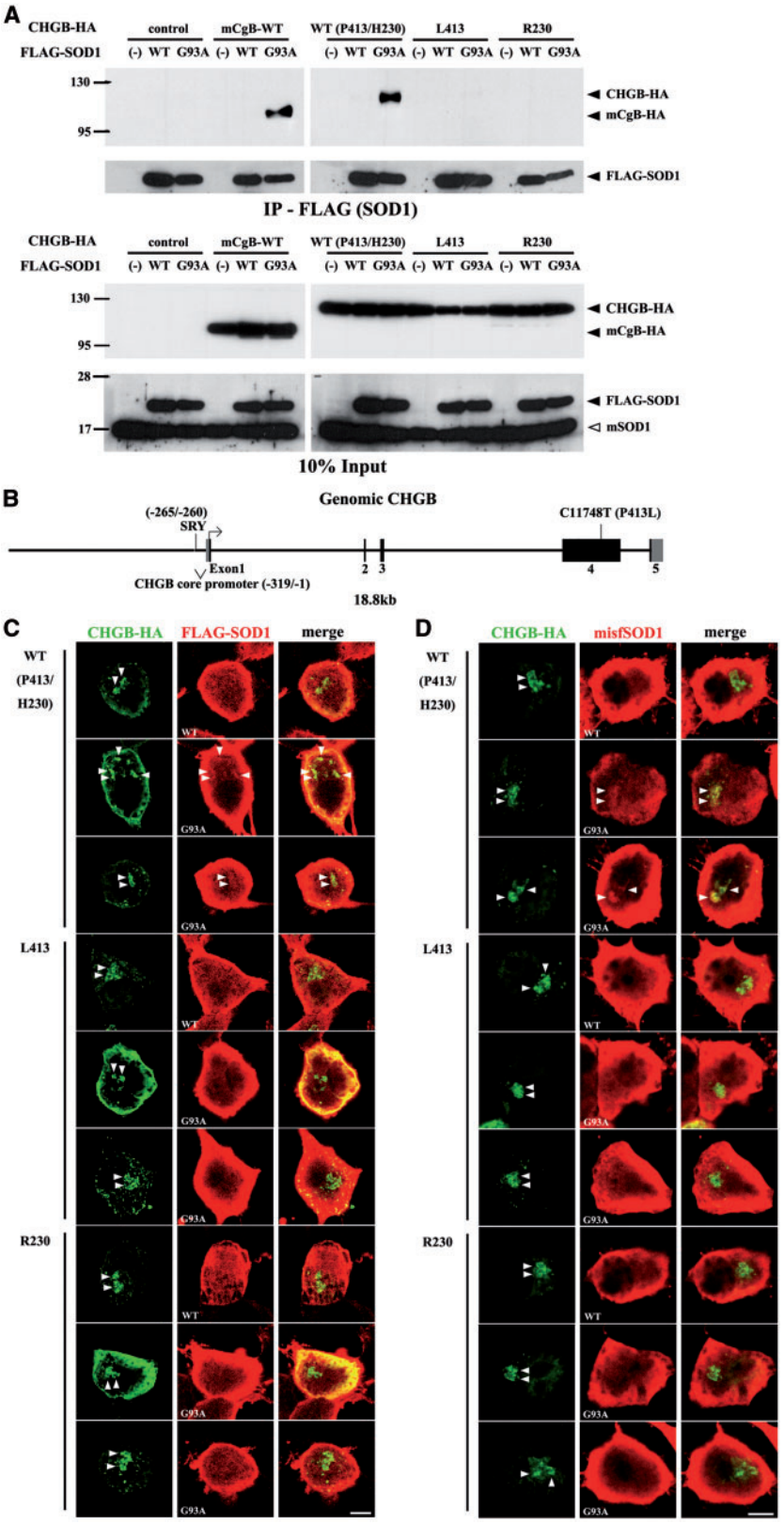

Figure 1. Defective binding of CHGB^{P413L} and CHGB^{H230R} variants to mutant SOD1 and misfolded SOD1 *in vitro*. (**A**) Defective interaction of CHGB^{P413L} and CHGB^{H230R} variants with mutant SOD1^{G93A} in cultured cells. Neuro2A cells were co-transfected with FLAG-tagged SOD1 and HA-tagged CHGB. Immunoprecipitates with anti-FLAG affinity gel (IP-FLAG) were immunoblotted using anti-HA or anti-SOD1 antibody. (**B**) DNA construct of genomic CHGB containing 5.1 kb of promoter and 13.7 kb of coding sequence. (**C, D**) Partial co-localization of mutant SOD1^{G93A} and misfolded SOD1 (misfSOD1) with WT CHGB in cultured cells but not with CHGB^{P413L} and CHGB^{H230R} variants. Neuro2a cells co-transfected with FLAG-SOD1 and HA-CHGB were immunostained using anti-HA and anti-FLAG (C) or anti-misfSOD1 antibodies (B8H10) (D). Arrowheads indicate CHGB accumulation and SOD1^{G93A} (C) or misfSOD1 (D) merged with CHGB. Scale bars, 10 μm.

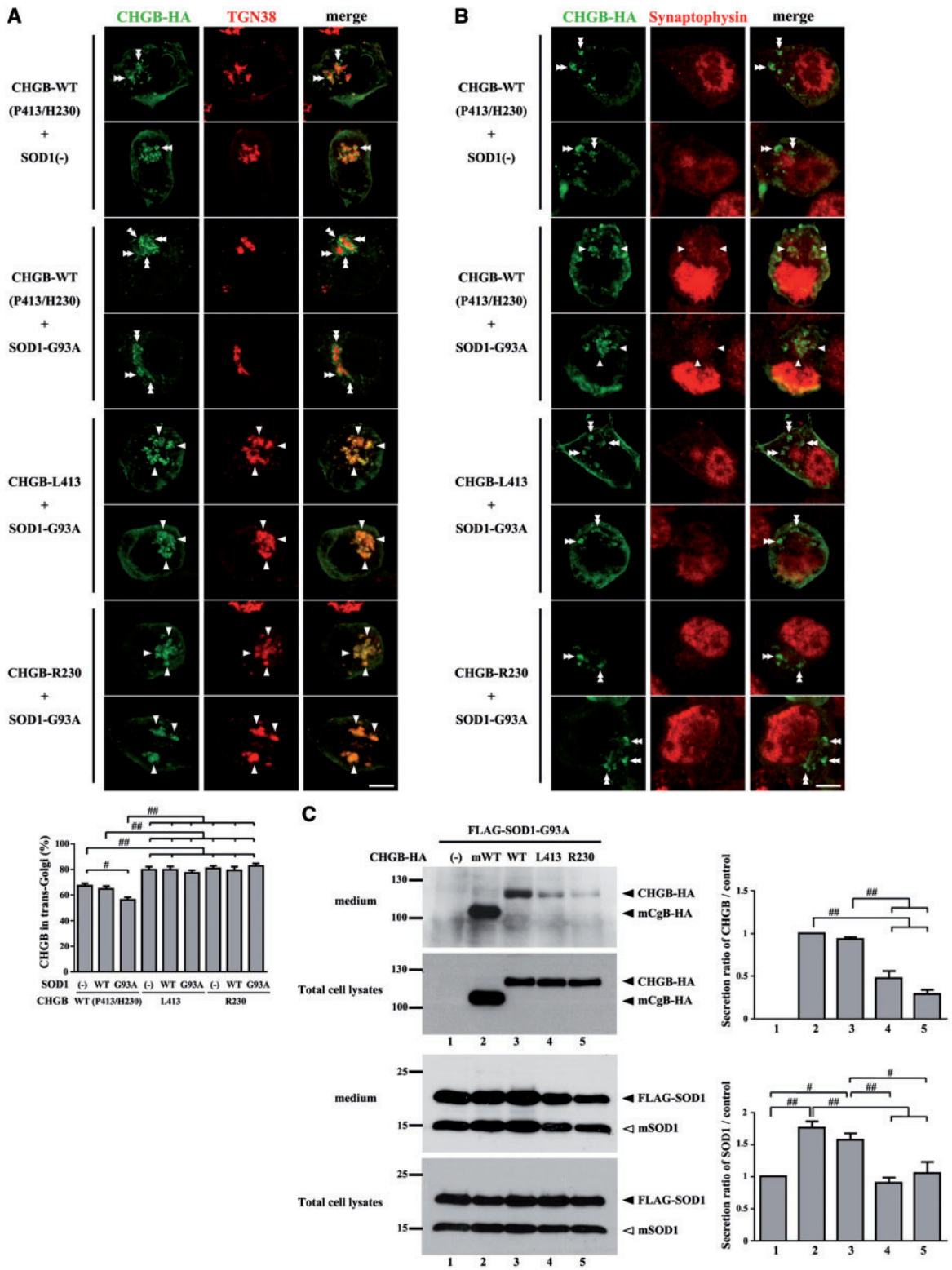

Figure 2. Mislocalization and secretion impairment of CHGB^{P413L} and CHGB^{H230R} variants *in vitro*. (**A**) Co-localization of the higher fractions of CHGB^{L413} and CHGB^{R230} variants with trans-Golgi marker (TGN38) in Neuro2a cells, with or without co-transfection with SOD1^{G93A}. Arrowheads indicate CHGB accumulation merged with TGN38. Double arrowheads indicate CHGB accumulation separated with TGN38. The percentages of CHGB vesicles merged with TGN-38 marker were analyzed. Data are mean ±SEM (N = more than 40 cells each). $^{\#}P < 0.05$, $^{\#\#}P < 0.01$ in post-ANOVA Turkey test (same for C). (**B**) Mis-localization of CHGB^{L413} and CHGB^{R230} variants with synaptic vesicles marker (synaptophysin) in context of SOD1^{G93A} expression. Arrowheads indicate CHGB accumulation merged with synaptophysin. Double arrowheads indicate CHGB accumulation not merged with synaptophysin. Scale bars, 10 μm. (**C**) Impaired promotion of CHGB^{L413} and CHGB^{R230} variants for mutant SOD1 secretion in cultured cells. Concentrated culture medium was immunoblotted using anti-HA or anti-SOD1 antibody. Densitometry of CHGB or SOD1^{G93A} were analyzed. The values (mean ±SEM, $N = 3$) represent the ratio compared to control (Lane 1 = control for SOD1, Lane2 = control for CHGB).

noteworthy that a higher fraction of the variants HA-CHGB^{L413} and HA-CHGB^{R230} (80%) were co-localized with trans-Golgi marker in Neuro2A cells, with or without co-transfection with SOD1^{G93A} (Fig. 2A). Moreover, unlike HA-CHGB WT, the variants HA-CHGB^{L413} and HA-CHGB^{R230} did not co-localized with the accumulation of synaptic vesicles in context of SOD1^{G93A} expression (Fig. 2B, double arrowheads). These results suggest a sorting of HA-CHGB WT to the secretory granules after leaving the trans-Golgi in Neuro2a cells, especially in context of mutant SOD1^{G93A} expression. In contrast, there was a defective sorting of HA-CHGB^{L413} and HA-CHGB^{R230} variants, which remained predominantly sequestered in trans-Golgi.

The mislocalization of HA-CHGB^{L413} and HA-CHGB^{R230} variants led us to further investigate the secretion of HA-CHGB and SOD1^{G93A} proteins after transfection of Neuro2A cells. After treatment of cells with stimulation buffer containing 2 mM $BaCl_2$ and 50 mM KCl, the amounts of CHGB^{L413} and CHGB^{R230} detected in the medium by western blot analysis were lesser than those of CHGB WT or of mouse CgB WT (Fig. 2C). Moreover, the expression of CHGB WT or mouse CgB promoted the secretion of mutant SOD1^{G93A} whereas variants CHGB^{L413} and CHGB^{R230} had no effect of the mutant SOD1 secretion. However, the expression of CHGB (WT, L413 and R230) and mouse CgB did not promote the secretion of endogenous mouse SOD1 in cells (data not shown).

Defective neurite outgrowth of cultured Neuro2A cells expressing variants CHGB^{L413} and CHGB^{R230}

Since previous studies demonstrated a role for CHGB in supporting neurite outgrowth of cultured cells (34–36), we examined the effects of CHGB^{L413} and CHGB^{R230} expression on neurite outgrowth of Neuro2a cells. Compared to control cells and to cells expressing CHGB WT (CHGB$^{P413/H230}$), a high percentage of cells expressing the variants CHGB^{L413} or CHGB^{R230} exhibited a decreased number of neurites and with neurites of shorter length (Supplementary Material, Fig. S2).

Overexpression of CHGB^{L413} transgene precipitated disease onset in SOD1^{G37R} female mice

To investigate whether CHGB variants might influence disease onset and duration in an animal model of ALS, we generated SOD1^{G37R} mice overexpressing either CHGB^{P413} or CHGB^{L413} transgenes. This was done by the breeding of SOD1^{G37R} mice with transgenic mice bearing CHGB^{P413} or CHGB^{L413} genomic fragments (18.8 kb) that included the CHGB promoter, introns and 3' sequences (Fig. 1B). We selected CHGB^{P413} or CHGB^{L413} transgenic mouse lines that overexpressed human CHGB mRNA species at similar levels in the spinal cord as assessed by quantitative real time RT-PCR. These transgenic mice also exhibited similar excess CHGB protein levels in the microsomal fraction of the spinal cord when examined at 210 days of age (Supplementary Material, Fig. S3A). The single CHGB^{P413} or CHGB^{L413} transgenic mice reproduced well and did not exhibit overt phenotypes during aging. However, we noticed that the CHGB^{L413} transgene, unlike the CHGB^{P413} transgene, was not transmitted in females with the expected Mendelian ratio of 50% (Supplementary Material, Table S1). Instead, the breeding of heterozygous CHGB^{L413} transgenic mice with C57BL6 mice yielded only 37% of offspring females carrying the *CHGB*^{L413} transgene.

The single SOD1^{G37R} mice as well as doubly transgenic SOD1^{G37R};CHGB^{P413} mice and SOD1^{G37R};CHGB^{L413} mice were monitored during aging by the rotarod score and body weight. The non-transgenic mice and single transgenic mice CHGB^{P413} and CHGB^{L413} showed no deficiency on the rotarod test or on body weight loss until 500 days of age (data not shown). The disease onset, as defined by 30% loss of maximum recorded time on rotarod (37,38), occurred at mean age of 365.7 ± 3.0 days in SOD1^{G37R};CHGB^{L413} mice, at 385.5 ± 1.1 days in SOD1^{G37R};CHGB^{P413} mice and at 394.5 ± 1.4 days in SOD1^{G37R} mice (Fig. S3B). Furthermore, we have stratified the tested group of mice according to their sex status and determined whether sex had an effect of disease onset by analyzing rotarod performance. Surprisingly, in female SOD1^{G37R};CHGB^{L413} mice, the onset of motor dysfunction occurred earlier at mean age of 360.3 ± 5.8 days compared with 408.8 ± 2.0 days in G37R mice ($P = 0.0041$) and 393.2 ± 2.1 days in SOD1^{G37R};CHGB^{P413} mice (Fig. 3A). In contrast, in male SOD1^{G37R} mice, the disease onset was not affected by the CHGB transgenes (either L413 or P413) and it occurred at a similar age (SOD1^{G37R}, SOD1^{G37R};CHGB^{P413}, SOD1^{G37R};CHGB^{L413} mice: 380.2 ± 3.4, 373.4 ± 1.8, 371.7 ± 6.7 days, respectively).

The CHGB^{L413} transgene increased ALS disease duration in female SOD1^{G37R} mice

Overexpression of CHGB^{L413} transgene did not affect survival of SOD1^{G37R} mice, whereas overexpression of *CHGB*^{P413} reduced survival of SOD1^{G37R} mice by 46 to 37 days in females and males, respectively (Fig. 3B, Supplementary Material, Figure S3C). As shown in Figure 3C and Supplementary Material, Figure S3D, the *CHGB*^{L413} transgene increased ALS disease duration in female SOD1^{G37R} mice, but not in males. In contrast, overexpression of *CHGB*^{P413} did not affect disease onset but it reduced survival and disease duration in both female and male SOD1^{G37R} mice. The data in Figure 3D, Supplementary Materials, Figures S3E and F revealed that the overexpression of CHGB^{L413} exacerbated the decline of motor performance on the rotarod test at disease onset in female SOD1^{G37R} mice. In contrast, overexpression of CHGB^{P413} exacerbated the decline of motor performance on rotarod test and of body weight at late stage of disease in SOD1^{G37R} mice.

The variant *CHGB*^{L413} transgene increased levels of misfolded SOD1 and exacerbated muscle denervation in female SOD1^{G37R} mice

To investigate whether overexpression of CHGB species was accompanied by an enhanced neuroinflammatory response in the lumbar cords of SOD1^{G37R} mice, lumbar cord sections at the end stage of disease were immunostained with anti-Mac2 antibody or anti-GFAP antibody. Enhanced microgliosis (Mac-2) was detected in SOD1^{G37R};CHGB^{P413} mice when compared to single SOD1^{G37R} transgenic mice (Fig. 4A). However, no such increase in microgliosis occurred in the SOD1^{G37R};CHGB^{L413} mice. There was no evidence of enhanced astrogliosis (GFAP) due to expression of either CHGB^{P413} or CHGB^{L413} in SOD1^{G37R} mice (Supplementary Material, Fig. S4). To investigate the degeneration of spinal α-motor neurons, lumbar cord sections at 345 days of age were immunostained with both anti-ChAT and anti-NeuN antibody. The number of α-motor neurons, which were positive for both ChAT and NeuN, in SOD1^{G37R};CHGB^{L413} and SOD1^{G37R};CHGB^{P413} mice at 345 days of age was similar to age-matched SOD1^{G37R} mice (Fig. 4B). A most

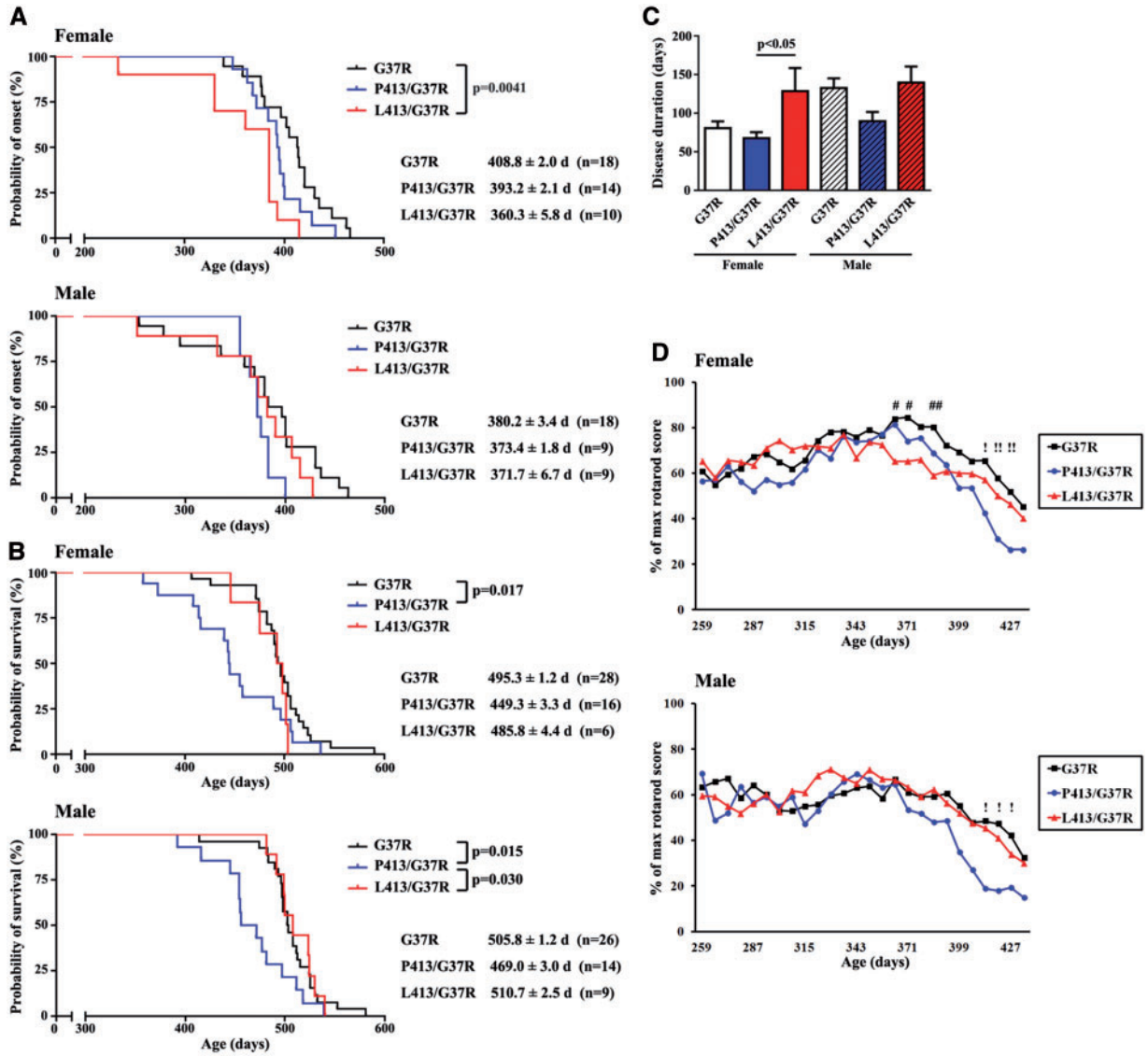

Figure 3. Early disease onset in SOD1^{G37R} female mice overexpressing CHGB^{L413} transgene. (A) Accelerated disease onset in SOD1^{G37R};CHGB^{L413} female mice but not in males. (B) Accelerated disease progression in both sexes of SOD1^{G37R};CHGB^{P413} mice but not in SOD1^{G37R};CHGB^{L413} mice. Kaplan-Meier survival analysis and the log-rank test were used (A, B). (C) Increased ALS disease duration in SOD1^{G37R};CHGB^{L413} female mice but not in males. Post-ANOVA Turkey test was used in each sex. (D) The decline of motor performance on rotarod test at disease onset due to overexpression of CHGB^{L413} in SOD1^{G37R} female mice and at late stage of disease due to overexpression of CHGB^{P413} in both sexes of SOD1^{G37R} mice. Data are mean ± SEM. $^{\#}P < 0.05$, $^{\#\#}P < 0.01$ between SOD1^{G37R} and SOD1^{G37R};CHGB^{L413},! $P < 0.05$,!! $P < 0.01$ between SOD1^{G37R} and SOD1^{G37R};CHGB^{P413} in post-ANOVA Turkey test.

striking change at this age was the reduced size of α-motor neurons in SOD1^{G37R};CHGB^{L413} female mice (Fig. 4B).

The levels of misfolded SOD1 species were determined in spinal cord extracts at end stage of disease by immunoprecipitation with anti-misfSOD1 antibody called B8H10 (33). The overexpression of CHGB^{P413} or CHGB^{L413} proteins enhanced the levels of misfSOD1 in SOD1^{G37R} mice (Fig. 4C). This effect was more pronounced in female than male mice (Fig. 4C). The neuromuscular junctions of gastrocnemius muscles were examined at 345 days of age. It is noteworthy that female SOD1^{G37R};CHGB^{L413} mice, but not males, exhibited higher denervation than SOD1^{G37R} mice or SOD1^{G37R};CHGB^{P413} mice (Fig. 4D). These results are consistent with a precipitation of disease onset in female SOD1^{G37R};CHGB^{L413} mice as determined by the rotarod test (Fig. 3A and D) whereas the enhanced microgliosis and misfSOD1 level in female SOD1^{G37R};CHGB^{P413} mice are consistent with a precipitation of disease progression (Fig. 3B).

Expression of CHGB^{L413} enhanced ER stress in female SOD1^{G37R} mice

As accumulation of misfSOD1 is known to induce ER stress in motor neurons of ALS (39,40), we examined the effects of variants CHGB^{L413} and CHGB^{R230} on ER stress and unfolded protein response (UPR). First, we analyzed Neuro2a cells co-transfected with CHGB and SOD1 vectors for ER stress. As shown in Figure 5A, expression of CHGB^{L413} or CHGB^{R230} variants caused an up-regulation of ER stress markers (Bip, pPERK, CHOP, cleaved cas-

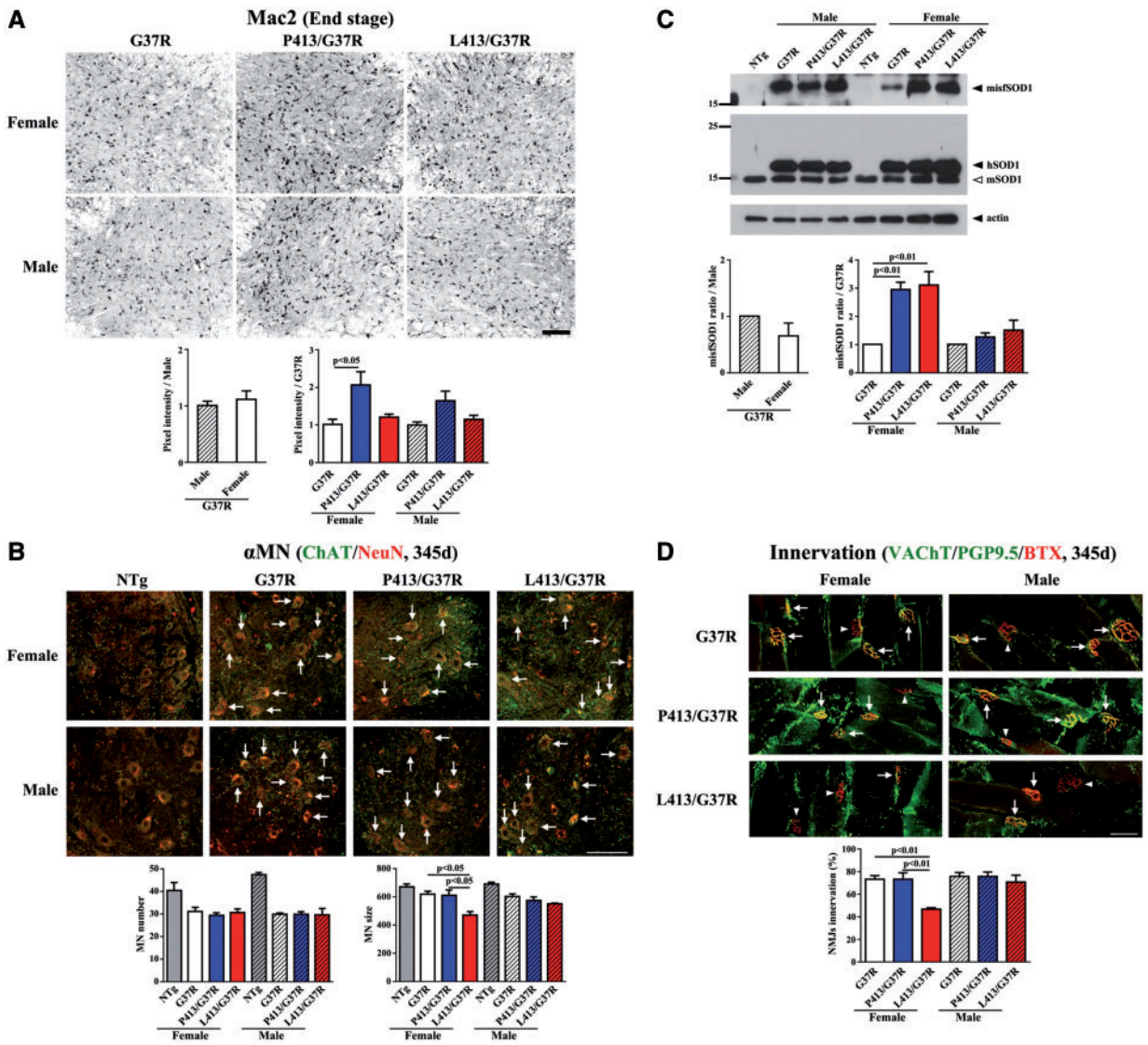

Figure 4. Enhanced levels of misfolded SOD1 and increased denervation in SOD1^{G37R} female mice overexpressing CHGB^{L413} transgene. (**A**) Enhanced microgliosis in SOD1^{G37R};CHGB^{L413} female mice at end stage. Signal intensities of Mac2 in five lumbar cord sections from each mice ($N = 3$–4) was analyzed. The values (mean ±SEM) represent the ratio compared to control (G37R mice). Post-ANOVA Turkey test was used in each sex (same for all figures). (**B**) The reduced sizes of α-motor neurons (α-MNs) in SOD1^{G37R};CHGB^{L413} female mice at 345 days of age. The number and size of motor neurons expressing both ChAT and NeuN were analyzed. Scale bars, 100 μm. (**C**) Enhanced levels of misfSOD1 in SOD1^{G37R};CHGB^{L413} and SOD1^{G37R};CHGB^{P413} female mice compared to SOD1^{G37R} female mice at end stage. Immunoprecipitates with misfSOD1 antibody (B8H10) was immunoblotted using anti-SOD1 antibody. Densitometry of misfolded SOD1 were analyzed ($N = 3$). (**D**) The extent of denervation in SOD1^{G37R};CHGB^{L413} female mice at 345 days of age. The Innervated (arrows) and denervated (arrow heads) neuromuscular junctions (NMJs) of gastrocnemius muscles was analyzed (100 NMJs from each mice, $N = 3$). Scale bars, 50 μm.

pase 12 (C12)) detected by Western blotting. Oxidative stress has been reported to induce unfolding of the SOD1 protein (32). Second, immunofluorescence analysis using spinal cord sections from single and double transgenic mice at 345 days of age was also carried out in order to confirm misfSOD1 and ER stress enhancement. The immunodetection of both misfSOD1 (C4F6 antibody) and Bip in motor neurons was enhanced in double SOD1^{G37R};CHGB^{L413} transgenic mice compared to single SOD1^{G37R} mice. Note that the induction was more robust in female mice (Fig. 5B, C and D). In contrast, expression of CHGB^{P413} did not enhance levels of misfSOD1 or ER stress (Bip) in motor neurons (Fig. 5B, C and D). To further confirm that CHGB^{L413} can exacerbate ER stress, the cytosolic/microsome fractions of mouse spinal cords (300 days of age) were immunoblotted with anti-CHGB antibody after immunoprecipitation with goat anti-SOD1 antibody (Santa Cruz). As expected, CHGB was co-immunoprecipitated with mutant SOD1 in fractions from SOD1^{G37R};CHGB^{P413} mice but not from SOD1^{G37R};CHGB^{L413} mice (Fig. 5E). Immunoblotting using anti-Bip antibody showed that CHGB^{L413} expression resulted in higher levels of Bip in cytosolic/microsome fractions of SOD1^{G37R} mice, especially females.

CHGB expression levels are higher in females than males

Interestingly, the immunoblotting results in Figure 5E and Supplementary Material, Figure S5A revealed higher levels of mouse CgB and human CHGB proteins in female mice than in male mice. This sex-dependent CHGB expression was further

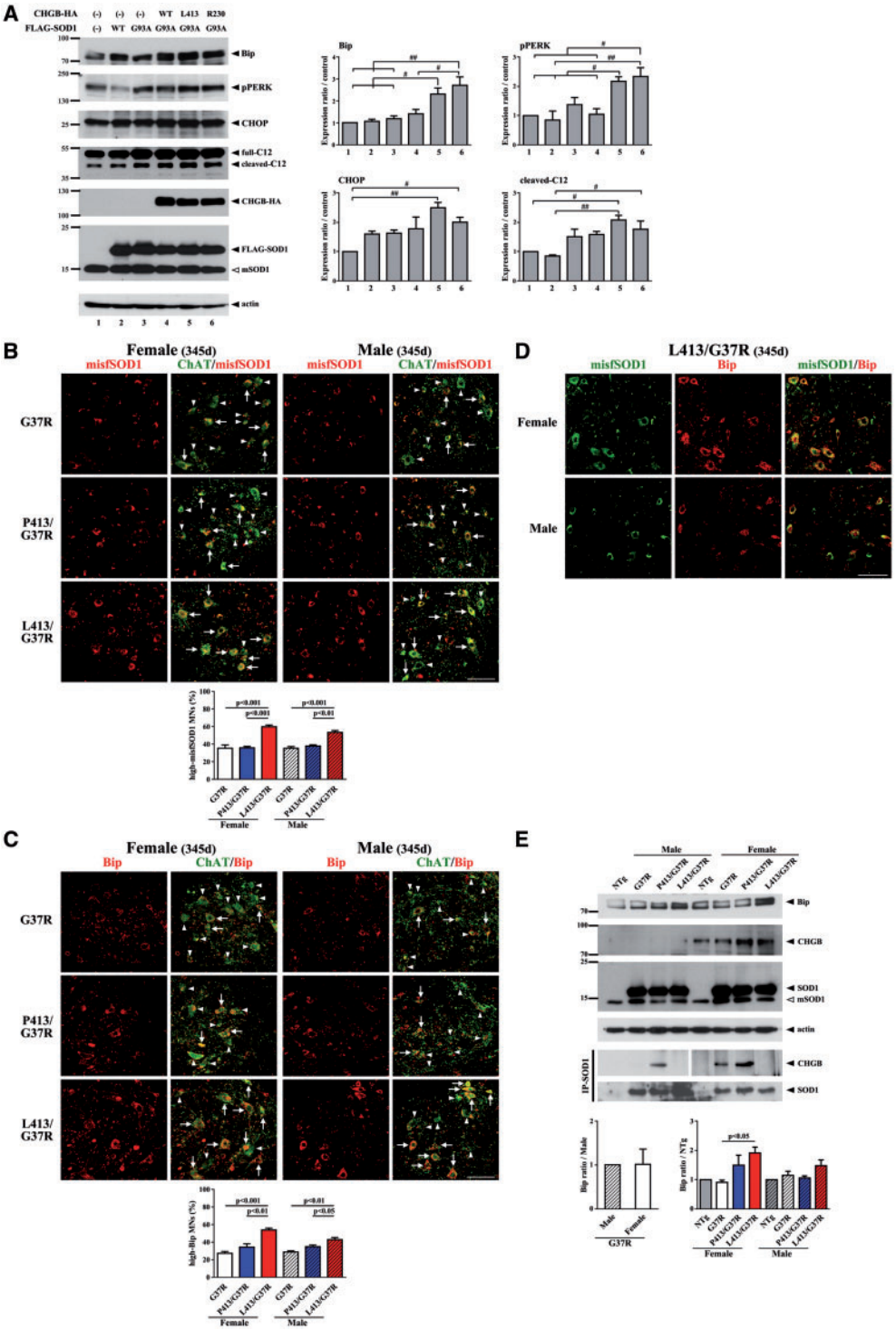

Figure 5 Enhanced ER stress in SOD1^{G37R} female mice overexpressing CHGB^{L413} transgene. (**A**) Enhanced ER stress due to oxidized SOD1^{G93A} by overexpression of CHGB^{P413L} and CHGB^{H230R} variants in cultured cells. After exposure to H_2O_2, the extranuclear fractions of Neuro2a cells co-transfected with FLAG-SOD1 and HA-CHGB were immunoblotted. Densitometry of the ER stress markers were analyzed. The values (mean ±SEM, $N = 3$) represent the ratio compared to control (Lane 1). $^{\#}P < 0.05$, $^{\#\#}P < 0.01$ in post-ANOVA Turkey test. (**B, C**) Accumulation of misfSOD1 (C4F6 antibody) (B) and Bip (C) in motor neurons of SOD1^{G37R};CHGB^{L413} mice especially females at 345 days of age. Numbers of motor neurons high (arrows) or low (arrow heads) expressing misfSOD1 (B) and Bip (C) signals in five lumbar cord sections from each mice ($N = 3$-4) was analyzed. Data are mean ±SEM. Post-ANOVA Turkey test was used in each sex (same for all figures). (**D**) Enhanced Bip expression due to misfSOD1 accumulation (C4F6 antibody) in motor neurons of SOD1^{G37R};CHGB^{L413} mice especially females at 345 days of age. Scale bars, 100 μm. (**E**) High expression of Bip in SOD1^{G37R};CHGB^{L413} female mice and CHGB proteins in SOD1^{G37R};CHGB^{L413} and SOD1^{G37R};CHGB^{P413} female mice at 300 days of age. The cytosolic/microsomal fractions of spinal cords were immunoblotted and the immunoprecipitates with anti-SOD1 antibody were immunoblotted. Densitometry of Bip were analyzed. The panels have been spliced for the IP-SOD1 results of male and female samples because results were obtained from two distinct immunoprecipitation experiments for male and female samples. The values (mean ±SEM, $N = 3$) represent the ratio compared to control (G37R male or non-Tg (NTg) mice) (see also Supplementary Material, Fig. S5A).

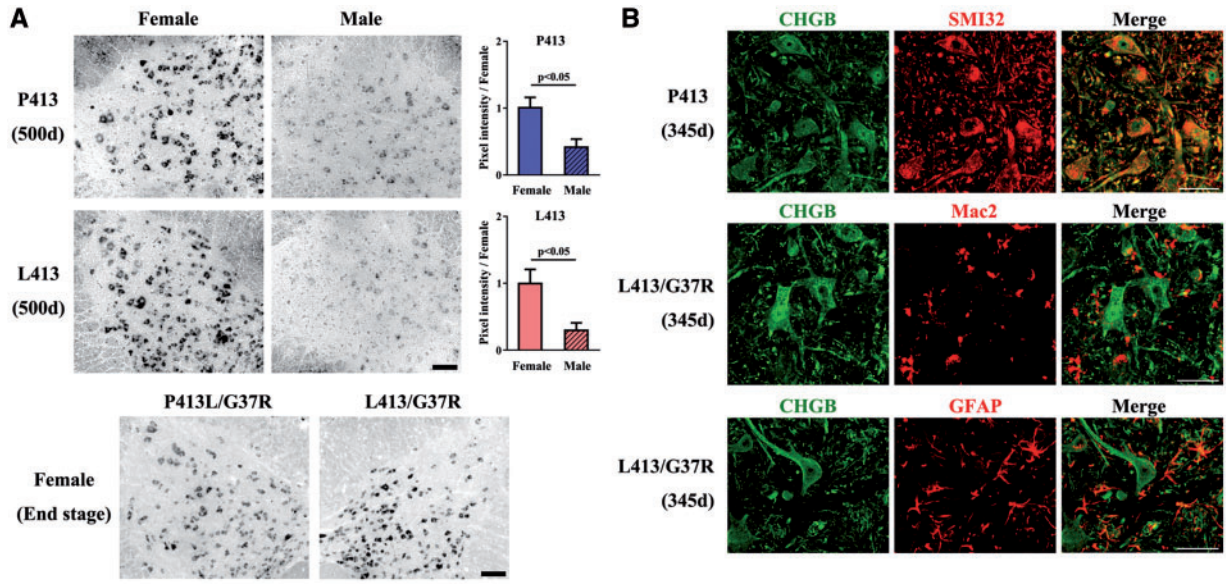

Figure 6. Higher neuronal expression of *CHGB* transgenes in female mice than male mice. (**A**) Higher expression levels of CHGB mRNA in the spinal cord of CHGB female mice compared to male mice. The lumbar cords of $CHGB^{P413}$ and $CHGB^{L413}$ mice and $SOD1^{G37R}$;$CHGB^{P413}$ and $SOD1^{G37R}$;$CHGB^{L413}$ female mice were analyzed by *in situ* hybridization. The signals of CHGB in seven lumbar cord sections from each mice ($N = 3$) was analyzed. The *t*-test was used for the values (mean ±SEM) representing the ratio compared to females. Scale bars, 100 μm. (**B**) CHGB expression occurs in neurons (SMI-32, neurofilament marker) not in glial cells of CHGB mice. Scale bars, 50 μm.

investigated by *in situ* hybridization on mouse spinal cord using an antisense probe for CHGB mRNA which did not interact with endogenous mCgB mRNA (Supplementary Material, Fig. S5B). As shown in Figure 6A, the CHGB mRNA levels were significantly higher in females than in males. The CHGB mRNA and CHGB protein species were expressed in neurons and not in glial cells of either single or double transgenic mice (Fig. 6A and B).

The $CHGB^{P413L}$ variant is a modifier of ALS onset for women in some populations

The results of sex dependent effects of $CHGB^{L413}$ variant for ALS onset in transgenic mice (Fig. 3A) led us to further investigate the effect of $CHGB^{L413}$ variant as a sex dependent disease modifier of ALS onset in Japanese population (Supplementary Material, Table S2). There was no significant difference in the age of onset between the $CHGB^{L413}$ and $CHGB^{P413}$ carriers in Japanese ALS patients (62.4 ± 0.3 years and 63.8 ± 0.1 years, respectively). However, further analyses of this Japanese cohort revealed important sex differences in the ALS onset of the L413 variation. As shown in Figure 7A, Japanese ALS female patients carrying the L413 variant showed an earlier age of ALS disease onset compared to those carrying the P413 variant (62.1 ± 0.7 years and 68.4 ± 0.3 years, respectively). In contrast, Japanese men with ALS carrying the L413 variant showed the same age of ALS onset as P413 carriers (62.6 ± 0.5 years and 61.4 ± 0.2 years, respectively).

The results with this Japanese population led us to re-analyze as a function of $CHGB^{L413}$ variant in the age of ALS onset in French-Canadian (26) (Supplementary Material, Table S2) as well as French (27) and Swedish (26) populations. Remarkably, ALS female patients of French-Canadian origin carrying the L413 variant exhibited an onset of disease over a decade before those carrying the P413 variant (49.9 ± 0.8 years and 61.3 ± 0.2 years, respectively) (Fig. 7B). In contrast, the L413 variation had only little effect on age of disease onset in men of French-Canadian origin having ALS (56.0 ± 0.2 years and 60.6 ± 0.1 years, respectively). The results from cohorts of Japan and French-Canada origins demonstrated sex-dependent effects of the $CHGB^{L413}$ variant on ALS onset. However, the L413 variation had no effect on disease onset in ALS cohorts from French (29) or Swedish (26) origins (Fig. 7C and D).

We further investigated the effect of the $CHGB^{L413}$ variant for ALS progression in a Swedish FALS family with two patients homogenous for the D90A/D90A SOD1 (Table 1) (41,42). A female patient is heterozygous for the Q258/L413 *CHGB* variants and has a remarkably slow progression rate: in 2016, she is alive with a documented disease history of 28 years and an ALSFRS of 24/40, making her one of the longest surviving ALS patients known. The patient is not taking riluzole and is not using mechanical ventilatory support. However, contrasting this, her sister died of respiratory failure 18 years after onset. The sister carried the common WT (R258/P413) CHGB alleles (Table 1). This family observation is in line with *CHGB* variants acting as disease modifiers of ALS progression as presented in *SOD1*-transgenic mice (Fig. 3B).

Discussion

The results presented here demonstrate sex-dependent effects of the allelic variant $CHGB^{P413L}$ on onset of ALS. The overexpression of $CHGB^{L413}$ transgene in $SOD1^{G37R}$ mice precipitated disease onset specifically in female mice, but not in male mice (Fig. 3A). Furthermore, sex-dichotomous effects of the $CHGB^{P413L}$ variation on ALS onset were also observed in Japanese and French-Canadian origin populations (Fig. 7A and B). Hence, women carrying the $CHGB^{L413}$ variation exhibited an earlier onset of disease compared to those carrying only the $CHGB^{P413}$ alleles in these ALS populations. The $CHGB^{L413}$ variation had only minor effect on age of disease onset in ALS men. Although there was no mutant *SOD1*-FALS in our Japanese and

Table 1. Association of the P413L variation with slower disease progression in Swedish ALS sisters carrying homogenous D90A SOD1

Patient No.	Sex	Genotype		Age of onset	Disease duration
		CHGB	SOD1		
466	F	R258Q/P413L	D90A/D90A	50 years	27 years (alive)
473	F	WT/WT	D90A/D90A	50 years	7 years

CHGB, chromogranin B; SOD1, superoxide dismutase 1.

French-Canadian subjects, an involvement of SOD1-mediated pathogenic mechanism is a possibility because aggregates of misfolded SOD1 species have regularly been detected in both sporadic ALS (SALS) and familial ALS (FALS) patients (43–45), and not only in neurons but also in glia cells (46). Moreover, $CHGB^{P413L}$ variant may cause other neuronal dysfunction such as secretion impairment, ER stress and neurite outgrowth defects (Figs. 2 and 5, Supplementary Material, S2) that can increase neuronal vulnerability to ALS pathogenesis. Anyhow, the sex-specific effect of the $CHGB^{P413L}$ variation in SALS was replicated in a mouse model bearing a FALS-linked *SOD1* mutant gene. The most plausible explanation for the sex-specific influence of $CHGB^{P413L}$ in ALS pathogenesis is that CHGB RNA and protein expression levels are higher in females than males (Figs. 5E and 6A, Supplementary Material, S5A). Indeed, there is an SRY element in the *CHGB* promoter that may act as a suppressor of transcription in males (Fig. 1B). It has been reported that the *SRY* on chromosome Y acts on the SRY region of the *CHGB* promoter reducing its activity (47). We find that SRY is immunodetected in spinal cord neurons of male mice (Supplementary Material, Figure S5C). Moreover, SRY is expressed in neurons of the brain and spinal cord of men and of male mice according to the gene expression data in the Allen Brain Atlas (http://www.brain-map.org). SRY has been reported to regulate directly catecholamine synthesis and metabolism in the midbrain (48,49). A search for sequence homologies revealed that the sequence of HMG-box region, which interacts to the SRY region of *CHGB* promoter, showed high homology between mouse and human SRY (Supplementary Material, Table S3). These results suggest that the mouse SRY can interact with the SRY region in the promoter of a human CHGB transgene to reduce its expression. Accordingly, a higher expression of *CHGB* occurred in females transgenic mice as determined by *in situ* hybridization with the antisense probe specific for CHGB (Fig. 6A).

From these results, we conclude that higher expression levels of *CHGB* in female $SOD1^{G37R}$ mice account for the sex-dichotomous effects of $CHGB^{P413L}$ variation in precipitating disease onset, ER stress induction and loss of neuromuscular junctions (Figs. 3A, 4D, 5B–E). Surprisingly, the overexpression of the $CHGB^{L413}$ transgene precipitated disease onset without affecting survival of $SOD1^{G37R}$ mice (Fig. 3A and B). In contrast, overexpression of $CHGB^{P413}$ transgene did not affect disease onset but it reduced survival of $SOD1^{G37R}$ mice (Fig. 3A–C). How to explain the differential effects of $CHGB^{L413}$ and $CHGB^{P413}$ genes on ALS pathogenesis in the mouse model? Our results demonstrate that $CHGB^{P413}$ protein can interact with mutant and misfSOD1 to enhance secretion of misfSOD1 (Fig. 1 and 2C). Accordingly, increasing the levels of extracellular misfSOD1 would increase microgliosis with ensuing motor neuron damage (27). Because of sex differences in *CHGB* expression levels, the microgliosis in the $SOD1^{G37R}$;$CHGB^{P413}$ mice was more prominent in females than males (Fig. 4A). Enhanced microgliosis is expected to influence disease progression without affecting disease onset (50). Therefore, enhanced secretion of misfSOD1 may explain why overexpression of $CHGB^{P413}$ proteins accelerated disease progression after onset. Conversely, the $CHGB^{L413}$ variant, which is unable to bind and to stimulate secretion of misfSOD1 in the milieu (Fig. 1 and 2C), enhanced disease onset suggesting that it may exert toxicity within motor neurons to enhance disease susceptibility (50). Accordingly, expression of $CHGB^{L413}$ in transfected Neuro2A cultured cells caused secretion defects and impaired neurite outgrowth (Fig. 2C, Supplementary Material, Figure S2). Moreover, expression of the $CHGB^{L413}$ transgene in female $SOD1^{G37R}$ enhanced the loss of neuromuscular junctions (Fig. 4D), and it increased ER stress and misfolded SOD1 levels in spinal motor neurons (Fig. 5). The overexpression of $CHGB^{L413}$ transgene prolonged disease duration in female $SOD1^{G37R}$ mice compared to female bearing the $CHGB^{P413}$ transgene (Fig. 3C). An association of *CHGB* variants with very long disease duration was also observed in ALS sisters homozygous for the $SOD1^{D90A}$ mutation (Table 1).

In summary, the results presented here suggest that *CHGB* variant alleles, the rare $CHGB^{L413}$ and common $CHGB^{P413}$, may act as modifiers of ALS disease dependent on their expression levels which is higher in females because of a sex-determining region Y element in the CHGB gene promoter. Expression of $CHGB^{L413}$ variant in $SOD1^{G37R}$ mice precipitated disease onset (Fig. 3A), but it also slowed down disease progression likely by restraining neuronal secretion of misfolded SOD1 in the milieu thereby attenuating microgliosis (Figs. 2C, 3B and C, 4A). In contrast, expression of the common $CHGB^{P413}$ allele in $SOD1^{G37R}$ mice exacerbated disease progression after onset most likely by increasing secretion of misfolded SOD1 and ensuing microgliosis (Figs. 2C, 3B and C, 4A). In view of the distinct modifier effects of the common and rare CHGB variants on ALS pathogenesis caused by *SOD1* mutation, it would be of interest to further investigate whether CHGB allelic variants might act as sex-modifiers in the ALS disease caused by other gene mutations and in TDP-43 proteinopathies. Since the L413 variation had no effect on disease onset in French and Swedish ALS cohorts unlike Japanese and French Canadian cohorts (Fig. 7), the divergent results might be explained by population-specific effects. Additional examinations of the L413 variation for other ALS populations will be needed to confirm this point.

Materials and Methods

Antibodies

The following antibodies were used in this study: anti-FLAG (M2, Sigma Aldrich, St. Louis, MO), anti-HA (H6908, Sigma;3F10, Roche, Mannheim, Germany), anti-SOD1 (SOD100, Enzo Life Science, Farmingdale, NY; C17, Santa Cruz Biotechnology, Santa Cruz, CA), anti-chromogranin B (26102, QED Bioscience, San Diego, CA; PA1-10839, Thermo, Rockford, IL), B8H10 (33), C4F6 (37), anti-TGN38 (M290, Santa Cruz), anti-synaptophysin (D35E4, Cell signaling technology, Danvers, MA), anti- synaptotagmin V (46, Santa Cruz), anti-Akt1 (B1, Santa Cruz), anti-Mac2

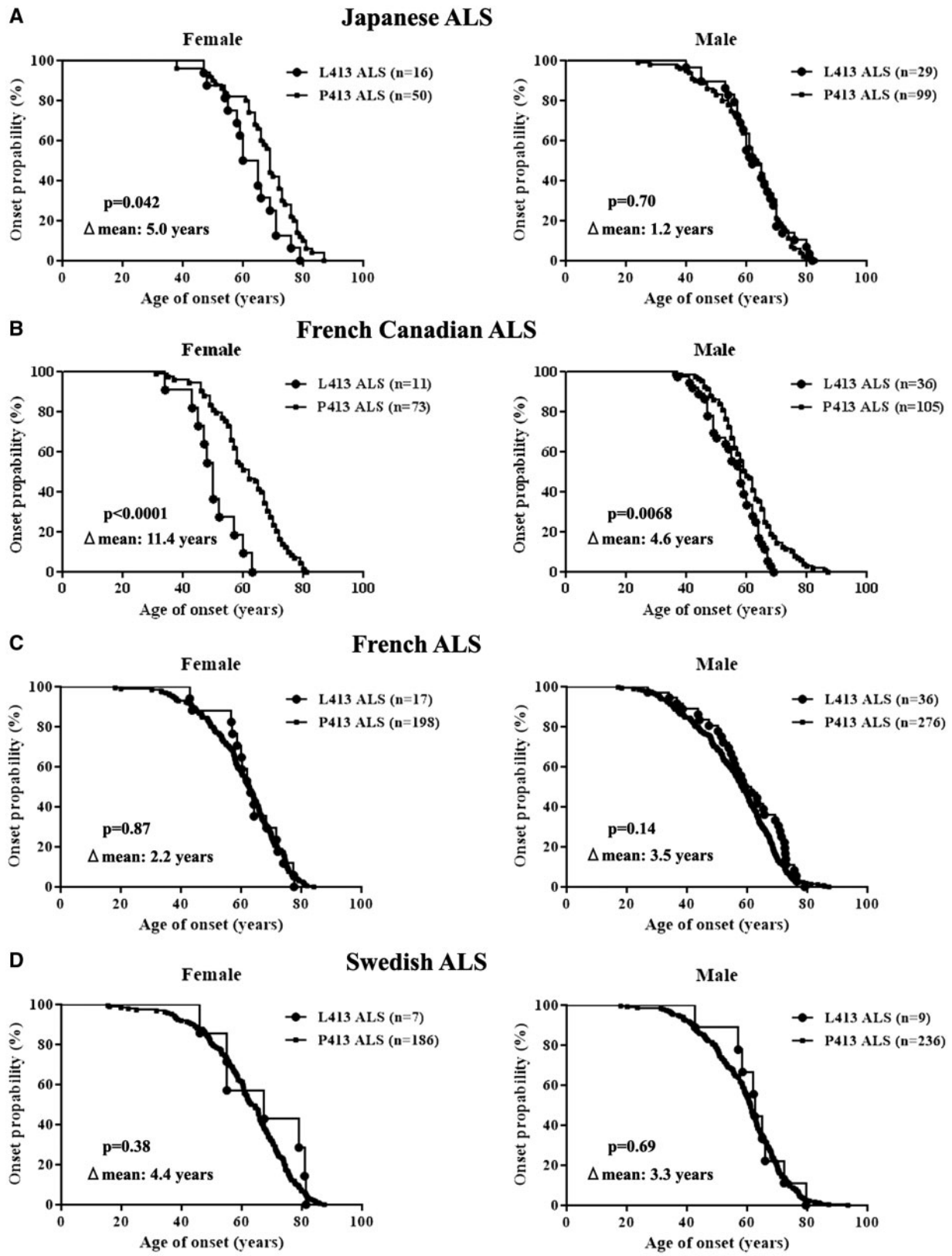

Figure 7. Earlier age of disease onset in women ALS carriers of the *CHGB*^{L413} variation from Japanese and French-Canadian cohorts. (**A**) The CHGB^{L413} variant was associated with an earlier age of onset compared to CHGB^{P413} variant in Japanese women with ALS but not in male ALS cases. (**B**) There was significant association of CHGB^{L413} variant with an earlier age of onset compared to CHGB^{P413} variant in French Canadian ALS cases, especially women. (**C, D**) However, there was no effect of the CHGB^{L413} variant on disease onset in cohorts of French (C) and Swedish (D) origins.

(hybridoma from ATCC, Rockville, MD, USA), anti-glial fibrillary acidic protein (GFAP) (GA5, Cell signaling), anti-choline acetyltransferase (ChAT) (AB144P, Millipore, Billerica, MA), anti-neuronal nuclear antigen (NeuN) (MAB5294, Millipore), anti-actin (Millipore), anti-human protein gene product 9.5 (PGP9.5) (7863-0504, AbD Serotec, Raleigh, NC), anti-vesicular acetylcholine transport (VAChT) (Milipore), rhodamine conjugated α-Bungarotoxin (Invitrogen, Carlsbad, CA), anti-Bip (3177, Cell Signaling; ab21685, abcam, Cambridge, MA), anti-phosphoprotein kinase-like endoplasmic reticulum kinase (PERK) (16F8, Cell Signaling), anti-C/EBP-homologous protein (CHOP) (F168, Santa Cruz), anti-caspase 12 (2202, Cell Signaling), SMI32 (Covance, Princeton, NJ), anti-SRY (E19, Santa Cruz).

Plasmids, cell culture and transfection

Mammalian expression plasmid carrying the human SOD1 (WT or G93A) tagged with FLAG (pcDNA3-FLAG-hSOD1), human CHGB (WT, P413L or H230R) tagged with HA (pcDNA3-CHGB-HA) were generated as previously described (27). The plasmid carrying CHGB fragment (P413 or L413) was generated (pBluescript-CHGB). Briefly, the human BAC clone RP11-518C18 containing the complete CHGB gene was used to amplify a 18.8 kb genomic fragment by PCR using a high fidelity polymerase (NEB). The CHGB fragment which contains promoter and coding sequence (exons and introns) was inserted into pBluescript. The P413L mutation was inserted into the genomic sequence using site-directed mutagenesis and the final clone was completely sequenced.

Murine neuroblastoma cell line, Neuro 2a cells were maintained in Dulbecco's modified essential medium (DMEM) containing 10% fetal bovine serum (27,32). Transfections were performed using Lipofectamin 2000 (Invitrogen) according to the manufacturer's protocol. At 24 h after transfection, the medium was replaced with the nutrient medium containing 5 mmol/l dibutyryl cAMP (Sigma) and antibiotics. At 48 h after transfection, cells were exposed to 1.5 mmol/l H_2O_2 for 30 min for the analysis of ER stress markers.

Subcellular fractionation of cultured cells

Following exposure to H_2O_2, cells were washed in cold PBS and then scrapped in cold PBS containing 1 mmol/l EDTA. The cells were harvested by centrifugation at 700 g for 5 min. After the centrifugation, the pellet was resuspended in a lysis buffer consisting of 10 mmol/l HEPES pH 8.0, 50 mmol/l NaCl, 0.1 mmol/l EDTA, 0.5 mol/l sucrose, 0.5% Triton X-100, protease inhibitor cocktail (Roche) and phosphatase inhibitor cocktail (Pierce Biotechnology) and incubated on ice for 5 min. The supernatants were centrifuged at 1,000 g for 10 min. After protein determination was performed by the Bradford method (Bio-Rad Laboratories, Hercules, CA), the supernatant was used as the extranuclear (cytosolic/membrane) fractions for the analysis of ER stress markers (51).

Immunoblotting and immunoprecipitation of cultured cells

At 48 h after transfection, cells were lysed in TNT-G buffer consisting of 50 mM Tris-HCl (pH 7.4), 150 mM NaCl, 10% glycerol, and 1% Triton-X100 with protease inhibitor cocktail (Roche). After 30 min incubation on ice, the cell suspension was centrifuged (20,000 g for 20 min) and the supernatant was collected. The cell lysates were incubated with anti-FLAG M2 agarose affinity gel (Sigma) at 4 °C overnight and were eluted with 4% SDS sample buffer (27). For the analysis of ER stress markers, the samples of subcellular fraction were used. Samples were resolved by SDS-PAGE and transferred to a PVDF membrane (Polyscreen, PerkinElmer, Boston, MA). A western blot image was obtained using a chemiluminescence detection kit (Pierce Biotechnology, Rockford, IL).

Immunocytochemistry

Cultured cells were fixed by 4% paraformaldehyde (PFA) for 30 min and cold Methanol for 20 min at room temperature, and were incubated with PBS containing 10% serum and 0.2% Triton-X100 for 1 h at room temperature for blocking. After blocking, cells were incubated with primary antibodies diluted in PBS containing 5% normal goat serum at 4°C overnight and subsequently with corresponding fluorescent secondary antibodies (Alexa, Invitrogen). Samples were observed by an investigator blinded to the genotype using confocal laser microscopy (FV300, Olympus, Tokyo, Japan) and the images were analyzed by the use of Image J.

The analyses of CHGB mislocalization and neurite outgrowth in cultured cells

For the calculation of CHGB percentages colocalizing with TGN-38 (trans-Golgi marker), the merged and unmerged CHGB vesicles with TGN-38 marker were analyzed. More than 40 cells were analyzed for each condition (28). For the analysis of the percentage of cells expressing neurites, average number of neurites per cell, and average length of neuritis, cells with neurites were defined as cells that possessed at least one neurite of greater than the diameter of the cell body (52–54). The data presented are the mean of three individual transfected 2 cm^2 dishes and are representative of three independent experiments. At least 100 cells per transfection were scored for neurite outgrowth.

Secretion assays

At 24 h after transfection, Neuro2a cells plated onto a 6-well culture dish were washed in PBS twice. Cells were incubated in basal secretion medium consisting of 10 mM HEPES, 129 mM NaCl, 5 mM NaHCO3, 4.8 mM KCl, 1.2 mM MgCl2, 1.2 mM KH2PO4, 1 mM CaCl2 and 2.8 mM glucose (pH 7.4) for 1 h, and then treated with 0.7 ml of secretagogue-containing medium (stimulation buffer: 10 mM HEPES, 79 mM NaCl, 5 mM NaHCO3, 50 mM KCl, 1.2 mM KH2PO4, 1.2 mM MgCl2, 2 mM BaCl2, 2.8 mM glucose, pH 7.4) for 15min (27). 500μl medium was collected and centrifuged for 5 min at 1,000g to remove the debris. The supernatants were concentrated by a protein concentrator with 10 kDa cut-off (Millipore), followed by western analysis. Secreted human (FLAG) or mouse SOD1, CHGB or CgB was estimated by standardization with intracellular human (FLAG) or mouse SOD1, CHGB or CgB in total cell lysates.

Animal models

All experimental procedures were carried out according to the Guide of Care and Use of Experimental Animals of the Canadian Council on Animal Care. The 18.8 kb full-length genomic fragments carrying *CHGB* (P413 or L413) (Fig. 1B) were microinjected

in 1-day-old mouse embryos. The founders were bred with non-transgenic C57BL/6 mice to establish stable transgenic lines. The genomic integration of the transgene was confirmed by PCR from mouse ear DNA. The mRNA in the spinal cord was analyzed by quantitative real-time PCR (qRT-PCR), as described below. One line with a highest copy of CHGB mRNA was maintained as C57BL/6.

The $SOD1^{G37R}$ (line 29) transgenic mice were a gift from Drs. P. Wong and D. Price from Johns Hopkins University (Baltimore, MD) and have been maintained as C57BL/6 in our laboratory (55). Double transgenic mice over-expressing CHGB species and mutant $SOD1^{G37R}$ were derived by breeding mice hemizygous for each of the *CHGB* generated transgene with $SOD1^{G37R}$ mice. The $SOD1^{G37R}$;CHGB mice were then genotyped by two sets of PCR primers for CHGB and $SOD1^{G37R}$ transgenes. The sequences of primers are shown in Supplementary Material, Table S4.

For clinical analyses, body weight and rotarod score were analyzed once a week starting at 200 days of age by investigators blinded to the genotype. The accelerating rotarod test was performed on mice at 4 rpm speed with 0.125 rpm/s acceleration. The length of time that mice stayed on the rod (up to a maximum of 4 min) was recorded as an indicator of grasping power. Three trials were performed and the best result was recorded. Using rotarod analysis, disease onset was determined as 30% loss of maximum recorded time (37,38). End-stage was defined as the time at which mouse could not right itself within 30 s when placed on its side.

Quantitative real time RT-PCR

Real-time RT-PCR was performed with a LightCycler 480 (Roche) sequence detection system using Light-Cycler SYBR green I at the Quebec Genomics Centre (56). Total RNA was extracted from frozen spinal cord tissues using Qiazol reagent (miRNeasy, Qiagen, Valencia, CA). Total RNA was treated with DNase (Qiagen) to get rid of genomic DNA contaminations. Total RNA was the quantified using Nanodrop, and its purity was verified by Bioanalyzer 2100 (Agilent Technologies, Mississauga, ON, Canada). Gene-specific primers were constructed using the GeneTools software (Biotools, Jupiter, FL). Two genes, Atp5o and 18S were used as internal control genes. The primers used for the analysis of genes are given in Supplementary Material, Table S4.

Immunofluorescence and immunohistochemistry of spinal cord and neuromuscular junction

Mice were anaesthetized and transcardially perfused with 0.9% NaCl and fixed with 4% paraformaldehyde (PFA) pH 7.4. Spinal cords and gastrocnemius muscles were dissected, post-fixed in 4% PFA pH 7.4 and then placed in phosphate-buffered saline (PBS)-sucrose 30% (55). Spinal cords or gastrocnemius muscles were cut on microtome or cryostat (Leica, Richmond Hill, ON, Canada) in 25 μm sections. Spinal sections were incubated with PBS containing 4% goat serum or bovine serum albumin and 0.3% Triton-X100 for 1h at room temperature for blocking. After blocking, sections were incubated with primary antibodies diluted in PBS at room temperature overnight and subsequently with corresponding fluorescent secondary antibodies (Alexa, Invitrogen) or with biotinylated secondary antibodies visualized by the avidin-biotin-immunoperoxidase complex (ABC) method using a Vectastain ABC kit (Vector Laboratories, Burlingame, CA) and 3,3'-diaminobenzidine tetrahydrochloride (DAB; Vector). Gastrocnemius muscle sections were incubated with PBS containing 4% bovine serum albumin and 0.3% Triton-X100 for 30min at room temperature for blocking. After blocking, sections were incubated with anti-PGP9.5 (1:500) and anti-VAChT (1:500) antibodies diluted in PBS at room temperature overnight and subsequently with corresponding fluorescent secondary antibodies (Alexa, Invitrogen) and rhodamine conjugated α-Bungarotoxin (1:1,000). Samples were microscopically video-captured or observed by confocal laser microscopy (LSM5 Pascal, Zeiss, Oberkochen, Germany). For the analysis of the number and size of α-motor neuron (MN) stained with both ChAT and NeuN and the semiquantitative evaluation of immunoractivity for Mac2 and GFAP, the average of number and size of α-MN and signal intensity in five lumbar cord sections from each mice ($n = 3$–4 mice for each group) was analyzed using Image J. For the analyses of denervation, 100 neuromuscular junctions from each mouse were analysed ($n = 3$ mice for each group). For the calculation of MN percentages expressing misfolded SOD1 or BiP, double positive MNs (MN markers was ChAT) and signal intensity values inside cells for the antigen of interest were calculated in five lumbar cord sections ($n = 3$–4 mice for each group) (57). Data of signal intensity were acquired using identical confocal settings.

Subcellular fractionation of the spinal cord lysates

Spinal cord tissues from CHGB transgenic mice were homogenized in a homogenization buffer consisting of 250 mM sucrose, 10 mM Tris-HCl (pH 7.4), 1 mM MgCl2 and protease inhibitor cocktail (27). The debris was excluded by centrifugation at 1,000 g for 15 min. After the pellet (mitochondrial fractions) was excluded by centrifugation at 8,000 g for 10 min, the supernatant (post-mitochondrial fractions) was ultracentrifuged at 100,000 *g* for 1 hr to separate into the supernatant (cytosolic fractions) and the pellet (microsome fractions). The pellet was lysed in the homogenization buffer containing 1% Triton X100 with brief osmication before protein determination.

Immunoblotting and immunoprecipitation of spinal cord lysates

The post-mitochondrial (cytoplasmic plus microsomal) fractions of spinal cords were prepared by the same protocol as subcellular fraction. B8H10 antibody (33) or anti-SOD1 polyclonal antibody (Santa Cruz) was bound to protein G-coated magnetic beads (Dyanl, Invitrogen, Camarillo) and was incubated with 50μg of spinal cords homogenized in TNG-T buffer or 150 μg of post-mitochondrial fractions of spinal cords overnight at 4°C (27). After washing, immunoprecipitates were eluted with SDS sample buffer. Immunoprecipitates were analyzed by Western blotting with SOD1-specific antibody (Enzo) or human CHGB (QED). Densitometries of misfSOD1 and Bip were analyzed using ImageJ and standardized with actin.

In situ hybridization of spinal cord

In situ hybridization procedures using digoxigenin-labelled cRNA probes for CHGB were performed as described previously (58). Bright field images of sections of the lumbar cord were used for quantification of CHGB overexpression within the gray matter. The average of signal intensity in seven sections from each mouse ($n = 3$ mice for each group) was analyzed using Image J.

Samples from study participants and genotyping

All participants were diagnosed by expert neurological clinicians and gave written informed consent. Diagnosis of ALS was made according to El Escorial criteria (59). Peripheral blood samples from Japanese SALS patients ($n = 141$) were collected in Okayama university. Those from ALS patients in Canada/Quebec (non-SOD1 FALS = 40, SALS = 249), France (SALS = 527) and in Swedish (FALS = 163, SALS = 290) were collected, as previously described (26,28,29). The *CHGB*^{P413L} were genotyped by restriction enzyme digestion, as previously described (28). Polymerase chain reaction (PCR) primer pairs were designed to amplify a 500-bp PCR fragment in which the P413L variation is located in the middle of the PCR fragment (5'- aacgtcagcatggccagtttag -3' and 3'- acaagttgggtatgatgctgggag -5'). P413L variation abolished an MspI restriction site. PCR fragments digested with MspI (New England BioLabs) were run on agarose gel to confirm the presence or absence of the P413L variation.

Data analysis

Data are expressed as means ± SEM. Statistical comparisons of data were performed using t-tests or one-way ANOVA followed by a Tukey-Kramer post hoc comparison. Kaplan-Meier survival analysis and the log-rank test were used for survival and comparison of onset. Statistical analyses were done using GraphPad Prism 5 (version 5.00; GraphPad Software, Inc., San Diego, CA). Statistical significance was set at $P < 0.05$.

Supplementary Material

Supplementary Material is available at *HMG* online.

Acknowledgements

We thank all the patients for their participation in the study. We thank Dr. Makoto Urushitani, Christine Bareil, Satsuki Kametaka and Dr. Zhuoran Sun for advices and technical assistance.

Conflict of Interest statement. None declared.

Funding

This work was supported by the Muscular Dystrophy Association (USA), Canadian Institutes of Health Research, and partly by Grand-in-Aid for Scientific Research (B) 2529320216, (C) 24591263, Challenging Research 24659651, and Grants-Aid from the Research Committees (Mizusawa H, Nakano I, Nishizawa M, Sasaki H, and Aoki M) from the Ministry of Health, Labour and Welfare of Japan. J.-P. J., F.G.L. and G.A.R. hold Canada Research Chair. Funding to pay the Open Access publication charges for this article was provided by the Canadian Institutes of Health Research.

References

1. Rosen, D.R., Siddique, T., Patterson, D., Figlewicz, D.A., Sapp, P., Hentati, A., Donaldson, D., Goto, J., O'Regan, J.P., Deng, H.X., *et al.* (1993) Mutations in Cu/Zn superoxide dismutase gene are associated with familial amyotrophic lateral sclerosis. *Nature*, **362**, 59–62.
2. Rosen, D.R. (1993) Mutations in Cu/Zn superoxide dismutase gene are associated with familial amyotrophic lateral sclerosis. *Nature*, **364**, 362.
3. DeJesus-Hernandez, M., Mackenzie, I.R., Boeve, B.F., Boxer, A.L., Baker, M., Rutherford, N.J., Nicholson, A.M., Finch, N.A., Flynn, H., Adamson, J., *et al.* (2011) Expanded GGGGCC hexanucleotide repeat in noncoding region of C9ORF72 causes chromosome 9p-linked FTD and ALS. *Neuron*, **72**, 245–256.
4. Renton, A.E., Majounie, E., Waite, A., Simon-Sanchez, J., Rollinson, S., Gibbs, J.R., Schymick, J.C., Laaksovirta, H., van Swieten, J.C., Myllykangas, L., *et al.* (2011) A hexanucleotide repeat expansion in C9ORF72 is the cause of chromosome 9p21-linked ALS-FTD. *Neuron*, **72**, 257–268.
5. Arai, T., Hasegawa, M., Akiyama, H., Ikeda, K., Nonaka, T., Mori, H., Mann, D., Tsuchiya, K., Yoshida, M., Hashizume, Y., *et al.* (2006) TDP-43 is a component of ubiquitin-positive tau-negative inclusions in frontotemporal lobar degeneration and amyotrophic lateral sclerosis. *Biochem. Biophys. Res. Commun.*, **351**, 602–611.
6. Chen, Y.Z., Bennett, C.L., Huynh, H.M., Blair, I.P., Puls, I., Irobi, J., Dierick, I., Abel, A., Kennerson, M.L., Rabin, B.A., *et al.* (2004) DNA/RNA helicase gene mutations in a form of juvenile amyotrophic lateral sclerosis (ALS4). *Am. J. Hum. Genet.*, **74**, 1128–1135.
7. Daoud, H., Valdmanis, P.N., Kabashi, E., Dion, P., Dupre, N., Camu, W., Meininger, V. and Rouleau, G.A. (2009) Contribution of TARDBP mutations to sporadic amyotrophic lateral sclerosis. *J. Med. Genet.*, **46**, 112–114.
8. Deng, H.X., Chen, W., Hong, S.T., Boycott, K.M., Gorrie, G.H., Siddique, N., Yang, Y., Fecto, F., Shi, Y., Zhai, H., *et al.* (2011) Mutations in UBQLN2 cause dominant X-linked juvenile and adult-onset ALS and ALS/dementia. *Nature*, **477**, 211–215.
9. Eymard-Pierre, E., Lesca, G., Dollet, S., Santorelli, F.M., di Capua, M., Bertini, E. and Boespflug-Tanguy, O. (2002) Infantile-onset ascending hereditary spastic paralysis is associated with mutations in the alsin gene. *Am. J. Hum. Genet.*, **71**, 518–527.
10. Fecto, F., Yan, J., Vemula, S.P., Liu, E., Yang, Y., Chen, W., Zheng, J.G., Shi, Y., Siddique, N., Arrat, H., *et al.* (2011) SQSTM1 mutations in familial and sporadic amyotrophic lateral sclerosis. *Arch. Neurol.*, **68**, 1440–1446.
11. Gitcho, M.A., Bigio, E.H., Mishra, M., Johnson, N., Weintraub, S., Mesulam, M., Rademakers, R., Chakraverty, S., Cruchaga, C., Morris, J.C., *et al.* (2009) TARDBP 3'-UTR variant in autopsy-confirmed frontotemporal lobar degeneration with TDP-43 proteinopathy. *Acta. Neuropathol.*, **118**, 633–645.
12. Greenway, M.J., Alexander, M.D., Ennis, S., Traynor, B.J., Corr, B., Frost, E., Green, A. and Hardiman, O. (2004) A novel candidate region for ALS on chromosome 14q11.2. *Neurology*, **63**, 1936–1938.
13. Hadano, S., Hand, C.K., Osuga, H., Yanagisawa, Y., Otomo, A., Devon, R.S., Miyamoto, N., Showguchi-Miyata, J., Okada, Y., Singaraja, R., *et al.* (2001) A gene encoding a putative GTPase regulator is mutated in familial amyotrophic lateral sclerosis 2. *Nat. Genet.*, **29**, 166–173.
14. Johnson, J.O., Mandrioli, J., Benatar, M., Abramzon, Y., Van Deerlin, V.M., Trojanowski, J.Q., Gibbs, J.R., Brunetti, M., Gronka, S., Wuu, J., *et al.* (2010) Exome sequencing reveals VCP mutations as a cause of familial ALS. *Neuron*, **68**, 857–864.
15. Kabashi, E., Valdmanis, P.N., Dion, P., Spiegelman, D., McConkey, B.J., Vande Velde, C., Bouchard, J.P., Lacomblez, L., Pochigaeva, K., Salachas, F., *et al.* (2008) TARDBP mutations in individuals with sporadic and familial amyotrophic lateral sclerosis. *Nat. Genet.*, **40**, 572–574.
16. Lambrechts, D., Storkebaum, E., Morimoto, M., Del-Favero, J., Desmet, F., Marklund, S.L., Wyns, S., Thijs, V., Andersson, J.,

van Marion, I., *et al.* (2003) VEGF is a modifier of amyotrophic lateral sclerosis in mice and humans and protects motoneurons against ischemic death. *Nat. Genet.*, **34**, 383–394.
17. Maruyama, H., Morino, H., Ito, H., Izumi, Y., Kato, H., Watanabe, Y., Kinoshita, Y., Kamada, M., Nodera, H., Suzuki, H., *et al.* (2010) Mutations of optineurin in amyotrophic lateral sclerosis. *Nature*, **465**, 223–226.
18. Nishimura, A.L., Mitne-Neto, M., Silva, H.C., Richieri-Costa, A., Middleton, S., Cascio, D., Kok, F., Oliveira, J.R., Gillingwater, T., Webb, J., *et al.* (2004) A mutation in the vesicle-trafficking protein VAPB causes late-onset spinal muscular atrophy and amyotrophic lateral sclerosis. *Am. J. Hum. Genet.*, **75**, 822–831.
19. Puls, I., Jonnakuty, C., LaMonte, B.H., Holzbaur, E.L., Tokito, M., Mann, E., Floeter, M.K., Bidus, K., Drayna, D., Oh, S.J., *et al.* (2003) Mutant dynactin in motor neuron disease. *Nat. Genet.*, **33**, 455–456.
20. Sreedharan, J., Blair, I.P., Tripathi, V.B., Hu, X., Vance, C., Rogelj, B., Ackerley, S., Durnall, J.C., Williams, K.L., Buratti, E., *et al.* (2008) TDP-43 mutations in familial and sporadic amyotrophic lateral sclerosis. *Science*, **319**, 1668–1672.
21. Van Deerlin, V.M., Leverenz, J.B., Bekris, L.M., Bird, T.D., Yuan, W., Elman, L.B., Clay, D., Wood, E.M., Chen-Plotkin, A.S., Martinez-Lage, M., *et al.* (2008) TARDBP mutations in amyotrophic lateral sclerosis with TDP-43 neuropathology: a genetic and histopathological analysis. *Lancet Neurol.*, **7**, 409–416.
22. Van Vught, P.W., Sutedja, N.A., Veldink, J.H., Koeleman, B.P., Groeneveld, G.J., Wijmenga, C., Uitdehaag, B.M., de Jong, J.M., Baas, F., Wokke, J.H., *et al.* (2005) Lack of association between VEGF polymorphisms and ALS in a Dutch population. *Neurology*, **65**, 1643–1645.
23. Wu, C.H., Fallini, C., Ticozzi, N., Keagle, P.J., Sapp, P.C., Piotrowska, K., Lowe, P., Koppers, M., McKenna-Yasek, D., Baron, D.M., *et al.* (2012) Mutations in the profilin 1 gene cause familial amyotrophic lateral sclerosis. *Nature*, **488**, 499–503.
24. Yang, Y., Hentati, A., Deng, H.X., Dabbagh, O., Sasaki, T., Hirano, M., Hung, W.Y., Ouahchi, K., Yan, J., Azim, A.C., *et al.* (2001) The gene encoding alsin, a protein with three guanine-nucleotide exchange factor domains, is mutated in a form of recessive amyotrophic lateral sclerosis. *Nat. Genet.*, **29**, 160–165.
25. Brenner, D., Muller, K., Wieland, T., Weydt, P., Bohm, S., Lule, D., Hubers, A., Neuwirth, C., Weber, M., Borck, G., *et al.* (2016) NEK1 mutations in familial amyotrophic lateral sclerosis. *Brain*, **139(Pt 5)**:e28. doi: 10.1093/brain/aww033.
26. Freischmidt, A., Wieland, T., Richter, B., Ruf, W., Schaeffer, V., Muller, K., Marroquin, N., Nordin, F., Hubers, A., Weydt, P., *et al.* (2015) Haploinsufficiency of TBK1 causes familial ALS and fronto-temporal dementia. *Nat. Neurosci.*, **18**, 631–636.
27. Urushitani, M., Sik, A., Sakurai, T., Nukina, N., Takahashi, R. and Julien, J.P. (2006) Chromogranin-mediated secretion of mutant superoxide dismutase proteins linked to amyotrophic lateral sclerosis. *Nat. Neurosci.*, **9**, 108–118.
28. Gros-Louis, F., Andersen, P.M., Dupre, N., Urushitani, M., Dion, P., Souchon, F., D'Amour, M., Camu, W., Meininger, V., Bouchard, J.P., *et al.* (2009) Chromogranin B P413L variant as risk factor and modifier of disease onset for amyotrophic lateral sclerosis. *Proc. Natl. Acad. Sci. U S A*, **106**, 21777–21782.
29. Blasco, H., Corcia, P., Veyrat-Durebex, C., Coutadeur, C., Fournier, C., Camu, W., Gordon, P., Praline, J., Andres, C.R. and Vourc'h, P. (2011) The P413L chromogranin B variation in French patients with sporadic amyotrophic lateral sclerosis. *Amyotroph. Lateral Scler.*, **12**, 210–214.
30. van Vught, P.W., Veldink, J.H. and van den Berg, L.H. (2010) P413L CHGB is not associated with ALS susceptibility or age at onset in a Dutch population. *Proc. Natl. Acad. Sci. U S A*, **107**, E77. author reply E78.
31. Claudia, R., Stefania, B., Francesca, A., Michele, B., Claudia, T., Fabio, G., Massimo, C., Christian, L. and Silvana, P. (2015) Lack of relationship between the P413L chromogranin B variant and a SALS Italian cohort. *Gene*, **568**, 186–189.
32. Ezzi, S.A., Urushitani, M. and Julien, J.P. (2007) Wild-type superoxide dismutase acquires binding and toxic properties of ALS-linked mutant forms through oxidation. *J. Neurochem.*, **102**, 170–178.
33. Gros-Louis, F., Soucy, G., Lariviere, R. and Julien, J.P. (2010) Intracerebroventricular infusion of monoclonal antibody or its derived Fab fragment against misfolded forms of SOD1 mutant delays mortality in a mouse model of ALS. *J. Neurochem.*, **113**, 1188–1199.
34. Chen, M., Tempst, P. and Yankner, B.A. (1992) Secretogranin I/chromogranin B is a heparin-binding adhesive protein. *J. Neurochem.*, **58**, 1691–1698.
35. Huttunen, H.J., Kuja-Panula, J. and Rauvala, H. (2002) Receptor for advanced glycation end products (RAGE) signaling induces CREB-dependent chromogranin expression during neuronal differentiation. *J. Biol. Chem.*, **277**, 38635–38646.
36. Jungling, S., Cibelli, G., Czardybon, M., Gerdes, H.H. and Thiel, G. (1994) Differential regulation of chromogranin B and synapsin I gene promoter activity by cAMP and cAMP-dependent protein kinase. *Eur. J. Biochem.*, **226**, 925–935.
37. Urushitani, M., Ezzi, S.A. and Julien, J.P. (2007) Therapeutic effects of immunization with mutant superoxide dismutase in mice models of amyotrophic lateral sclerosis. *Proc. Natl. Acad. Sci. U S A*, **104**, 2495–2500.
38. Drachman, D.B., Frank, K., Dykes-Hoberg, M., Teismann, P., Almer, G., Przedborski, S. and Rothstein, J.D. (2002) Cyclooxygenase 2 inhibition protects motor neurons and prolongs survival in a transgenic mouse model of ALS. *Ann. Neurol.*, **52**, 771–778.
39. Kanekura, K., Suzuki, H., Aiso, S. and Matsuoka, M. (2009) ER stress and unfolded protein response in amyotrophic lateral sclerosis. *Mol. Neurobiol.*, **39**, 81–89.
40. Saxena, S. and Caroni, P. (2011) Selective neuronal vulnerability in neurodegenerative diseases: from stressor thresholds to degeneration. *Neuron*, **71**, 35–48.
41. Andersen, P.M., Forsgren, L., Binzer, M., Nilsson, P., Ala-Hurula, V., Keranen, M.L., Bergmark, L., Saarinen, A., Haltia, T., Tarvainen, I., *et al.* (1996) Autosomal recessive adult-onset amyotrophic lateral sclerosis associated with homozygosity for Asp90Ala CuZn-superoxide dismutase mutation. A clinical and genealogical study of 36 patients. *Brain*, **119 (Pt 4)**, 1153–1172.
42. Andersen, P.M., Nilsson, P., Keranen, M.L., Forsgren, L., Hagglund, J., Karlsborg, M., Ronnevi, L.O., Gredal, O. and Marklund, S.L. (1997) Phenotypic heterogeneity in motor neuron disease patients with CuZn-superoxide dismutase mutations in Scandinavia. *Brain*, **120 (Pt 10)**, 1723–1737.
43. Bosco, D.A., Morfini, G., Karabacak, N.M., Song, Y., Gros-Louis, F., Pasinelli, P., Goolsby, H., Fontaine, B.A., Lemay, N., McKenna-Yasek, D., *et al.* (2010) Wild-type and mutant SOD1 share an aberrant conformation and a common pathogenic pathway in ALS. *Nat. Neurosci.*, **13**, 1396–1403.
44. Grad, L.I., Yerbury, J.J., Turner, B.J., Guest, W.C., Pokrishevsky, E., O'Neill, M.A., Yanai, A., Silverman, J.M.,

Zeineddine, R., Corcoran, L., *et al.* (2014) Intercellular propagated misfolding of wild-type Cu/Zn superoxide dismutase occurs via exosome-dependent and -independent mechanisms. *Proc. Natl. Acad. Sci. U S A*, **111**, 3620–3625.
45. Forsberg, K., Jonsson, P.A., Andersen, P.M., Bergemalm, D., Graffmo, K.S., Hultdin, M., Jacobsson, J., Rosquist, R., Marklund, S.L. and Brannstrom, T. (2010) Novel antibodies reveal inclusions containing non-native SOD1 in sporadic ALS patients. *PLoS One*, **5**, e11552.
46. Forsberg, K., Andersen, P.M., Marklund, S.L. and Brannstrom, T. (2011) Glial nuclear aggregates of superoxide dismutase-1 are regularly present in patients with amyotrophic lateral sclerosis. *Acta. Neuropathol.*, **121**, 623–634.
47. Zhang, K., Rao, F., Wang, L., Rana, B.K., Ghosh, S., Mahata, M., Salem, R.M., Rodriguez-Flores, J.L., Fung, M.M., Waalen, J., *et al.* (2010) Common functional genetic variants in catecholamine storage vesicle protein promoter motifs interact to trigger systemic hypertension. *J Am. Coll. Cardiol.*, **55**, 1463–1475.
48. Czech, D.P., Lee, J., Sim, H., Parish, C.L., Vilain, E. and Harley, V.R. (2012) The human testis-determining factor SRY localizes in midbrain dopamine neurons and regulates multiple components of catecholamine synthesis and metabolism. *J. Neurochem.*, **122**, 260–271.
49. Dewing, P., Chiang, C.W., Sinchak, K., Sim, H., Fernagut, P.O., Kelly, S., Chesselet, M.F., Micevych, P.E., Albrecht, K.H., Harley, V.R., *et al.* (2006) Direct regulation of adult brain function by the male-specific factor SRY. *Curr. Biol.*, **16**, 415–420.
50. Boillee, S., Yamanaka, K., Lobsiger, C.S., Copeland, N.G., Jenkins, N.A., Kassiotis, G., Kollias, G. and Cleveland, D.W. (2006) Onset and progression in inherited ALS determined by motor neurons and microglia. *Science*, **312**, 1389–1392.
51. Oh, Y.K., Shin, K.S., Yuan, J. and Kang, S.J. (2008) Superoxide dismutase 1 mutants related to amyotrophic lateral sclerosis induce endoplasmic stress in neuro2a cells. *J. Neurochem.*, **104**, 993–1005.
52. Biernat, J., Wu, Y.Z., Timm, T., Zheng-Fischhofer, Q., Mandelkow, E., Meijer, L., and Mandelkow, E.M. (2002) Protein kinase MARK/PAR-1 is required for neurite outgrowth and establishment of neuronal polarity. *Mol. Biol. Cell*, **13**, 4013–4028.
53. Bryan, B., Kumar, V., Stafford, L.J., Cai, Y., Wu, G. and Liu, M. (2004) GEFT, a Rho family guanine nucleotide exchange factor, regulates neurite outgrowth and dendritic spine formation. *J. Biol. Chem.*, **279**, 45824–45832.
54. Bryan, B.A., Cai, Y. and Liu, M. (2006) The Rho-family guanine nucleotide exchange factor GEFT enhances retinoic acid- and cAMP-induced neurite outgrowth. *J. Neurosci. Res.*, **83**, 1151–1159.
55. Ezzi, S.A., Lariviere, R., Urushitani, M. and Julien, J.P. (2010) Neuronal over-expression of chromogranin A accelerates disease onset in a mouse model of ALS. *J. Neurochem.*, **115**, 1102–1111.
56. Swarup, V., Phaneuf, D., Bareil, C., Robertson, J., Rouleau, G.A., Kriz, J. and Julien, J.P. (2011) Pathological hallmarks of amyotrophic lateral sclerosis/frontotemporal lobar degeneration in transgenic mice produced with TDP-43 genomic fragments. *Brain*, **134**, 2610–2626.
57. Saxena, S., Roselli, F., Singh, K., Leptien, K., Julien, J.P., Gros-Louis, F. and Caroni, P. (2013) Neuroprotection through excitability and mTOR required in ALS motoneurons to delay disease and extend survival. *Neuron*, **80**, 80–96.
58. Schaeren-Wiemers, N. and Gerfin-Moser, A. (1993) A single protocol to detect transcripts of various types and expression levels in neural tissue and cultured cells: in situ hybridization using digoxigenin-labelled cRNA probes. *Histochemistry*, **100**, 431–440.
59. Brooks, B.R., Miller, R.G., Swash, M. and Munsat, T.L. (2000) El Escorial revisited: revised criteria for the diagnosis of amyotrophic lateral sclerosis. *Amyotroph. Lateral Scler, Other Motor Neuron. Disord.*, **1**, 293–299.